Gamma-ray bursts, evolution of massive stars and star formation at high redshifts
ASI Conference Series, 2012, Vol. 5, pp 69 – 79
Edited by S. B. Pandey, V. V. Sokolov and Yu A. Shchekinov

Evidences of the central engine activity in the Naked-Eye Burst prompt optical emission

S. Karpov[1*], G. Beskin[1], S. Bondar[2], A. Guarnieri[3], C. Bartolini[3], G. Greco[4] and A. Piccioni[3]

[1]*Special Astrophysical Observatory, Nizhnij Arkhyz 369167, Russia*
[2]*Institute for Precise Instrumentation, Nizhnij Arkhyz 369167, Russia*
[3]*Astronomy Department of Bologna University, Bologna, Italy*
[4]*Astronomical Observatory of Bologna, INAF, Italy*

Abstract. Naked-Eye Burst is the only event to date observed in optical and gamma-ray energies simultaneously with sufficiently high temporal resolution. This opens unprecedented possibilities for testing various models of both emission generation and the central engine behavior during the burst. The temporal properties of the observed light curve, along with tight optical to gamma relation, suggest the intrinsic periodicity of internal engine, which is supposedly a newborn stellar-mass compact object surrounded by an unstable precessing massive accretion disk.

Keywords : gamma-ray bursts: individual (GRB 080319B)

1. Introduction

Long-duration gamma-ray bursts are supposedly produced by newborn compact relativistic objects, stellar-mass black holes or highly magnetized neutron stars, during the collapse of the core of massive stars (Piran 2005; Meszaros 2006). Multi-wavelength observations of the GRBs are important tools to study these objects, whose behavior defines the temporal structure of the bursts. Therefore, the discovery of prompt optical emission in follow-up observations (Akerlof et al. 1999; Vestrand et al. 2005; Yost et al. 2007; Page et al. 2007) has led to the refinement of different GRB models. However the insufficient temporal resolution of the observations, typically worse than 10 s, has prevented clarifying the nature of the bursts.

*email: karpov@sao.ru

In order to capture the initial moments of the burst optical emission with high temporal resolution, we have designed and built several wide-field monitoring cameras (Piccioni et al. 1993; Karpov et al. 2005; Molinari et al. 2006). One of these cameras, the TORTORA (Telescopio Ottimizzato per la Ricerca dei Transienti Ottici RApidi), has successfully carried out high temporal resolution observations of the Naked-Eye Burst, GRB 080319B (Karpov et al. 2008; Racusin et al. 2008; Beskin et al. 2008). This was – and still is – the first case study of a GRB's optical emission from the beginning till the end, with a resolution comparable to the one of gamma-ray observations. We discovered the fast variability of the optical emission and its lag behind the gamma-ray emission, which reflects the periodic activity of the burst internal engine – likely, a hyperaccreting solar-mass compact object formed in the collapse of a massive stellar core.

The aim of this paper is to describe the TORTORA observations and data reduction of GRB 080319B (Section 2), then to perform a detailed comparative analysis of the optical and gamma emission (Section 3), and finally to discuss the nature of the discovered optical emission and its variability (Section 4).

2. Observations

We observed the region of GRB 080319B from 30 minutes before the trigger time T, until several tens of minutes after (Karpov et al. 2008; Racusin et al. 2008), with TORTORA wide field (24×32 degrees) monitoring camera (temporal resolution 0.13 s) (Molinari et al. 2006) mounted on the REM telescope at La Silla (Chile). After receiving the coordinates of GRB 080319B communicated by the Swift satellite, the position of the burst was moved from the edge of the TORTORA field of view towards its center. Therefore from T + 24.5 s till T + 31 s the REM telescope performed an automatic re-pointing (see Fig. 1).

The acquired data were processed by the standard TORTORA pipeline including CCD dark current subtraction and flat-fielding. The reduction were performed by a customary code accomplishing circular aperture photometry and then verified by IRAF DAOPHOT code, except the data acquired during the REM re-pointing. Over that period of time, the target and nearby stars' images are stretched up to 5 times on the time scale of a single exposure due to the motion of the field of view.

Such motion significantly lowers the signal-to-noise ratio and makes it impossible to perform reliable flux measurements on every single frame. To overcome this challenge, we performed the summation of sets of 10 non-overlapping frames, spatially shifting them to compensate the motion of the telescope and to obtain profiles of the trails with a signal-to-noise ratio nearly equal to one in other intervals of the light curve (see Fig. 2c). Then we processed the co-added frames through a customary elliptic aperture photometry code as well as by means of PSF-fitting, which provided consistent results. The effective temporal resolution for this interval is 1.3 s. For all

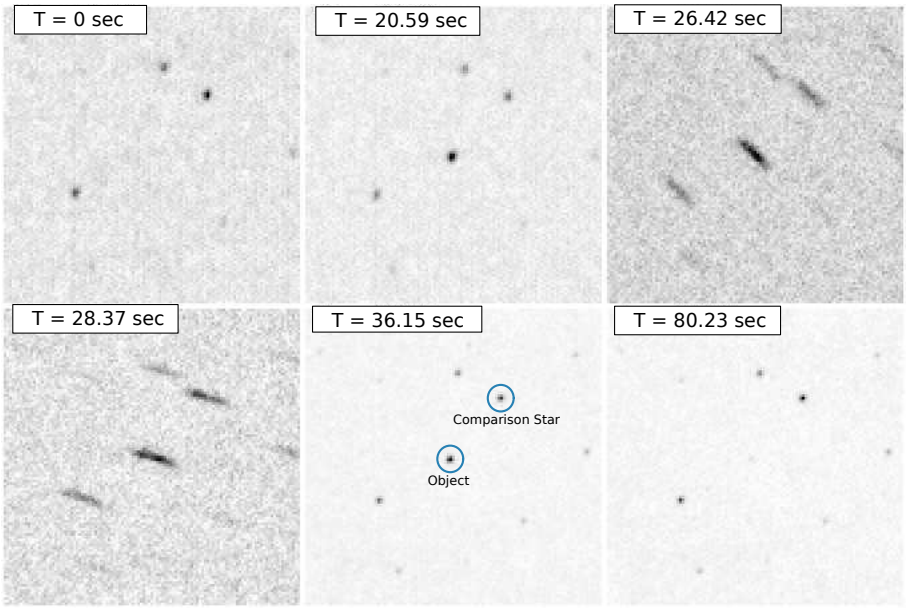

Figure 1. The development of prompt optical emission from GRB 080319b as seen by TORTORA camera. Sums of 10 consecutive frames with 1.3 s effective exposures are shown for the gamma-ray trigger time ($T = 0$ s), the maximum brightness time during the first peak ($T = 20.5$ s), two middle-part moments ($T = 26.4$ s and $T = 28.4$ s), at the last peak ($T = 36$ s) and during early afterglow ($T = 80$ s) stages. Image size is 2.5 x 2.5 degrees. Circles mark the transient (in the center) and the brightest of the nearest field stars used for photometric calibration, whose light curve is shown in Fig. 2b.

other time intervals the photometry has been performed with both full (0.13 s exposure) and low temporal resolution (1.3 effective exposure for 10 co-added images). Then, we obtained the instrumental magnitudes of the object, both for the REM repointing interval and the other parts of the light curve. These were calibrated to the Johnson V band using several nearby Tycho-2 stars. The light curve of one of the comparison stars, processed and calibrated in the same way as the transient, is shown in Fig. 2b. No significant deviation from the constant flux, neither in high resolution, nor in low resolution mode is present, which argues in favor of the real nature of variations seen in the light curve of the transient.

A quick-look low resolution light curve (excluding the data during the REM repointing interval) has been published (Karpov et al. 2008; Racusin et al. 2008). Our complete full resolution light curve, along with the low resolution one (after the restoring of the gap), is shown in Fig. 2.

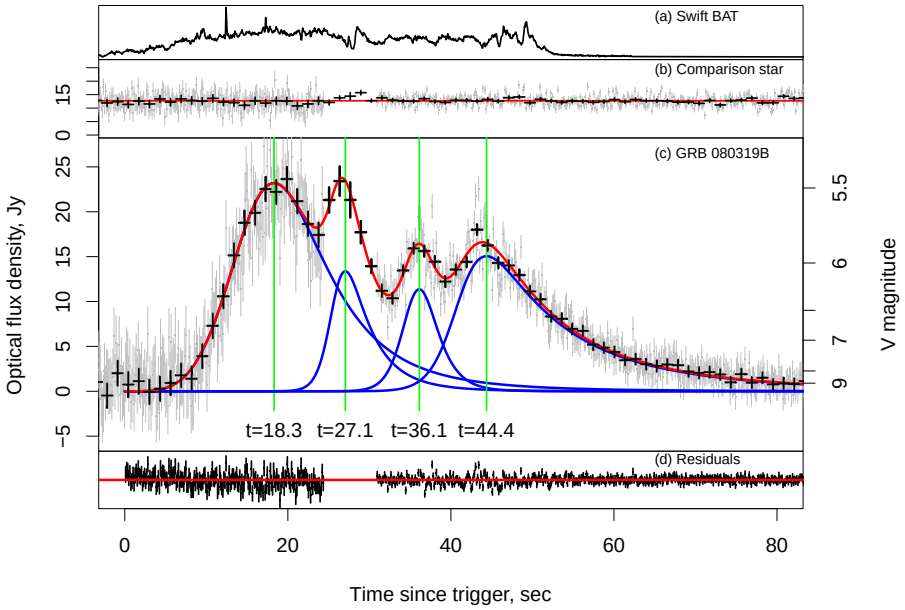

Figure 2. The light curve of GRB 080319B acquired by TORTORA wide-field camera (c), approximated by the sum of four peaks with parameters listed in Table 1. Residuals of such approximation are shown in (d). The gamma-emission, presented for comparison in (a), started at $T \approx -4$ s and faded at $T \approx 57$ s. The light curve of comparison star (b) shows no significant features.

3. Analysis of optical light curve

3.1 Periodicity of optical emission

The light curve of GRB 080319B clearly shows four peaks with similar amplitudes, durations and shapes (see Fig. 2c). We approximated the low-resolution data by the sum of four components described by a simple functions smoothly connecting two power laws (Kocevski et al. 2003)

$$F = F_0 \left(\frac{t}{T_0}\right)^r \left(\frac{d}{d+r} + \frac{r}{d+r}\left(\frac{t}{T_0}\right)^{r+1}\right)^{-(r+d)/(r+1)} \quad (1)$$

(where t is the time since trigger) whose parameters are listed in Table 1. The fit over the interval from $T = 0$ s till $T = 100$ s has a $\chi^2 = 33.4$ for 61 degrees of freedom. The distances between peaks are the same within the errors: $\Delta T \approx 8.5$ s in the observer frame, which corresponds to 4.4 s in the rest frame at $z = 0.937$ (Racusin et al. 2008; Beskin et al. 2008).

We then performed a Fourier analysis of the central part of the light curve (full-

Table 1. Best-fit parameters for the decomposition of the light curve into 4 peaks with shape described by Kocevski (Kocevski et al. 2003) profile (see Eq. 1), shown in Fig. 2c. Here, T_0 and F_0 are the peak maximum position relative to trigger time and flux, while r and d are the power-law indices of their rising and declining parts. ΔT is the distance between the peak and the next one.

T_0, s	F_0, Jy	r	d	$\Delta T, s$
18.3 ± 0.3	23.2 ± 0.6	4.0 ± 0.4	-5.4 ± 4.1	8.7± 0.4
27.0 ± 0.3	13.4 ± 3.4	24.8 ± 8.3	-9.7 ± 4.9	9.1± 0.4
36.1 ± 0.2	11.4 ± 1.7	25.9 ± 7.6	-22.0 ± 17	8.3± 0.5
44.4 ± 0.5	15.1 ± 1.8	21.9 ± 3.3	-5.1 ± 0.2	

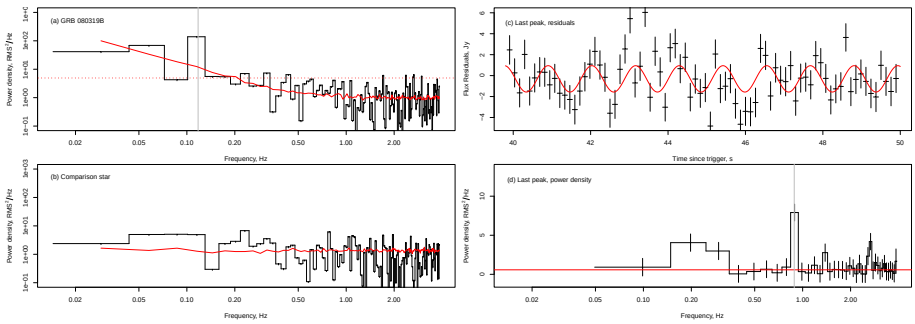

Figure 3. (a) Power density spectrum of plateau phase (since T + 14 s till T + 49 s) of the Naked-Eye Burst optical light curve with linear trend removed. (b) Power density spectrum of the same interval of bright nearby star light curve. (c) Optical flux for a T + 40 s – T + 50 s interval (last peak) with the approximation shown in Fig. 2 subtracted. (d) Power density spectrum of these data.

resolution one, with data points finely sampled with 0.13 s separation), defined as the interval between the first and the last peak extended by the mean distance between peaks, that is from $(T_1 - 0.5\Delta T) = 14.05$ s until $(T_4 + 0.5\Delta T) = 48.65$ s.

The power density spectrum of this light curve interval after removal of the linear trend is shown in Fig. 3a. A feature at $\nu_0 \approx 0.12$ Hz (marked by vertical line) is clearly visible and corresponds to the mean distance between the light curve peaks, alongside the low-frequency components of the overall two-level step-like structure of this part of the light curve (not completely compensated by linear trend removal).

Its significance, however, strongly depends on the assumed model of the shape of the underlying continuum component – the zero hypothesis. Reconstructing it from surrounding points, as an arithmetic mean of two nearest bins, gives a 24.5 times excess of the actual spectral density over the continuum (dotted horizontal line in Fig. 3a). Assuming the standard exponential probability distribution of power density

estimates over the mean value, it corresponds to $p = 3 \cdot 10^{-9}$ probability of zero hypothesis after correcting for the amount of 133 bins in the whole spectrum.

A more conservative estimate can be made modeling the un-detrended light curve with the sum of red and white noise components, approximating its spectral density excluding the bin containing the periodic component in question. We generated a large set of such processes and detrended each of them in the same way as the original data. The mean values of spectral density of such artificial data are shown as a smooth solid curve in Fig. 3a. The periodic feature then shows the 13.4 times excess over the mean zero-hypothesis level, which corresponds to a $p = 2 \cdot 10^{-4}$ significance level taking into account the full number of bins in the complete spectra (133 bins).

The power spectrum of the comparison star, derived in the same way and for the same light curve region, does not display any features with significance better than 0.01 in a single bin (0.35 for total number of 133 bins) in respect to mean noise level (see Fig. 3b), neither at the frequency of the peak seen in the transient spectrum, nor anywhere else. This rules out a possible artificial nature of the periodicity earlier discovered.

Thus, for the first time, we have a clear detection of periodic variations of a GRB prompt optical emission on a few seconds time-scale.

To study short time-scale optical variability, the smooth curve - formed by four fitted peaks - has been subtracted from the original full-resolution high-resolution data. The residuals are shown in Fig. 2d. The power spectral analysis of different sub-intervals of the burst revealed no signature of a variability in the 0.1-3.5 Hz (0.3-10 s) range with power exceeding 15% before and 10% after the REM re-pointing, except for the signature, marked by a vertical line in Fig. 3d, of a periodic intensity variation during the last peak, from $T + 40$ s till $T + 50$ s, with a 13.7 times excess over mean noise level (horizontal line in Fig. 3d), which implies a $p = 2.4 \cdot 10^{-5}$ significance for 39 bins. The period and amplitude of a best-fit sinusoidal approximation, shown in Fig. 3c, are 1.13 s and 9%, respectively. No other interval, neither of the object nor of the comparison stars light curves, shows any variability in the 0.1-3.5 Hz (0.3-10 s) range with power exceeding 15% before and 10% after the REM repointing (see Fig. 2d). The spectrum of gamma-ray light curve lacks the signature of such periodic variations on top of its stochastic variability, like the longer time scale one.

3.2 Correlation between optical and gamma-ray emission

In order to reveal the similarity between optical and gamma-ray light curves, and to filter out the stochastic variability of the latter, we performed a cross-correlation analysis. Again, we used solely the plateau phase of the light curves, excluding the first and last 12 seconds of the burst, both in optical and in gamma, as they are obviously highly correlated (Beskin et al. 2008). For the low-resolution data, with a 1.3

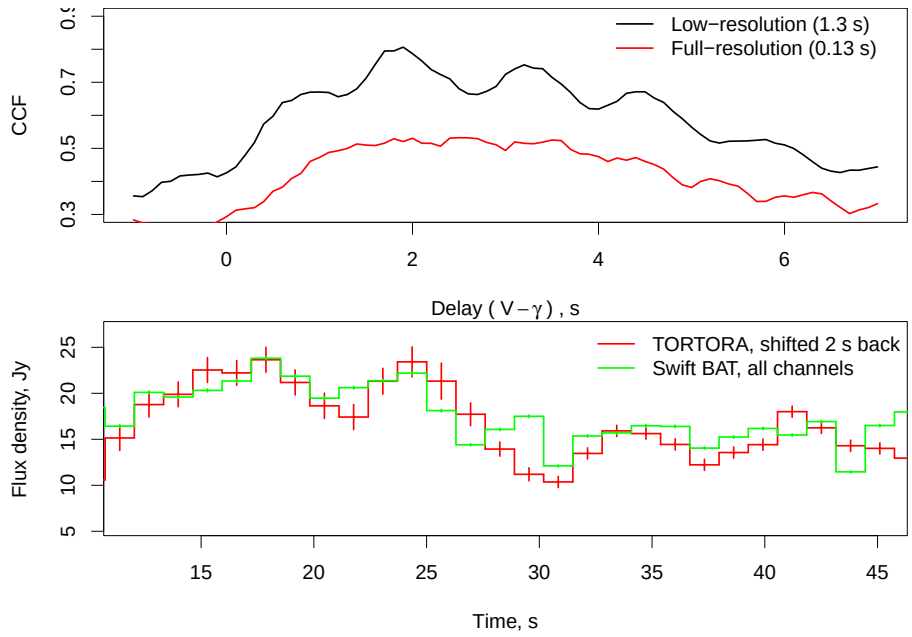

Figure 4. Upper panel – cross-correlation of the Swift-BAT gamma-ray (data from all energy channels with 64 ms temporal resolution) and TORTORA (data with 0.13 s and 1.3 s resolution) optical fluxes for the main (plateau) phase of the burst emission. Lower panel – TORTORA optical flux shifted back 2 seconds along with correspondingly re-binned Swift-BAT gamma-ray flux. Gamma-ray curve is arbitrarily scaled and shifted for illustrative purposes.

s bin size, the correlation coefficient is as high as 0.82 with a significance level of $5 \cdot 10^{-7}$ when the optical light curve is shifted 2 seconds back with respect to gamma-ray one (see Fig. 4). The correlation of unshifted data, at the same time, is as small as 0.42 with a significance of 0.03. Correspondingly re-binned gamma-ray data show the same four quasi-equidistant peaks as the optical ones (lower panel of Fig. 4). Correlation of high resolution data (0.13 s bin) is systematically lower due to higher amount of noise in it. Quasi-periodic variations of cross-correlation for low resolution data are due to a sharp feature in gamma-ray data at around $T + 30$ s falling into either one or two bins of re-binned light curve.

Nevertheless, the periodic variability components seen in the optical light curve are not manifested in the power density spectrum of the corresponding intervals of the gamma-ray one. This is most likely due to a significant amount of stochastic, shot noise-like variability of gamma emission which spans from tens to fractions of seconds (Margutti et al. 2008), possibly masking any low-amplitude regular structure in the data. Indeed, the non-stationary ejection of matter from the burst internal engine most likely modulates not the amplitudes of flares in the light curve, but their rate (see Section 4 and references therein) – and such modulation results in a complex transformation of underlying process power spectrum, presumably leaking the power

from periodic peaks. To study such a case we performed extensive set of simulations of "gamma-ray light curves" consisting of a short flares with varying rate (or mean distance between them) which tracks the smooth optical light curve intensity, and found that for nearly 90% of realizations the power spectra of simulated light curves do not show any features on the frequency in question, while keeping the correlation with optical light curve roughly as high as $r = 0.82$ observed. Obviously, there are other possible types of stochastic process modulation which may be revealed only in smoothed data, but not in the power spectrum.

4. Discussion

The $\Delta t \approx 2$ s delay of the optical flash relative to the gamma-ray one inevitably suggests that they were generated in different parts of the ejecta. More precisely, the optical photons came from a distance $\Delta R \approx 2c\Gamma^2\Delta t(1+z)^{-1} = 1.5 \cdot 10^{16}\Gamma_{500}^2$cm away from the central engine, where Γ_{500} is the Lorentz factor in units of 500 (Piran 2005; Li & Waxman 2008).

This result and other peculiarities we detected in the Naked-Eye Burst clearly contradict the proposed emission generation mechanisms based on various kinds of interactions between a single ensemble of electrons and photons they generate – synchrotron or inverse Compton ones (Racusin et al. 2008; Kumar & Panaitescu 2008; Fan & Piran 2008), the model of two internal shocks, forward and reverse (Yu, Wang & Dai 2009), and a relativistic turbulence model (Kumar & Narayan 2009). On the other hand, the fast rise and the similarity of durations of all four optical flashes rule out an external shock (both forward and reverse) as a source of optical emission (Zou, Piran & Sari 2009).

Two internal shock models have also been proposed, in which optical and gamma-ray flashes are generated by a synchrotron mechanism in different parts of the ejecta – the larger the photon energy, the closer it is to the central engine. These models are the residual collisions model (Li & Waxman 2008) and the model with significant input of neutron component (Fan, Zhang & Wei 2009). In these scenarios, the gamma emission is produced at a distance of 10^{14}-10^{15} cm from the center due to the electron heating caused by shock waves of colliding proton shells. In the former model, optical quanta are generated in an optically thin plasma during the collisions of "residual" shells (each shell being the result of the merging between a large number of thinner "original" shells), far ($\gtrsim 10^{16}$ cm) from the central engine (Li & Waxman 2008). In the latter model, the optical emission is generated by the electrons produced in β-decay of neutrons, which may reach a distance of $R \sim 10^{16}$ cm without interactions with other components of the ejecta. The decay products, protons and electrons, collide with faster proton shells ejected later, producing secondary internal shocks which heat the electrons generating synchrotron optical emission. Both models easily explain the two-second delay observed in the optical light curve, as well as its general smoothness on 0.1-1 s time scale, in contrast to high level of stochastic variability in

the gamma-ray emission (Margutti et al. 2008). On the other hand, the great difference of Naked-Eye Burst optical and gamma-ray fluxes ($F_o/F_\gamma \sim 10^3$) (Racusin et al. 2008) is more naturally explained in a neutron-rich model (Fan et al. 2009). As a matter of fact, a large amount of neutrons is unavoidable in bright gamma-ray bursts like GRB 080319B (Derishev, Kocharovsky & Kocharovsky 1999; Pruet, Woosley & Hoffman 2003). This model, therefore, is preferable, and our results may be a strong evidence of the existence of a significant neutron component in the ejecta.

In brief, we conclude that optical and gamma emission of Naked-Eye Burst were generated at different distances from the central engine. Such conclusion is a direct consequence of the detected similarity of shifted optical and gamma-ray light curves. Such similarity depends neither on particular mechanisms of conversion of mechanical to internal electron energy, nor on the emission mechanisms. Moreover, this effect can not be caused by the density or velocity variations inside the ejecta, such as those already observed on a time scale of several tens of minutes in afterglows of other gamma-ray bursts (Jakobsson et al. 2004; Bersier et al. 2003). Obviously, it would be impossible for the relativistic ejecta itself to display similar structures and dynamics, especially periodic behaviors, in regions separated by 10^{16} cm. Therefore, we have to conclude that these variations have the same cause – namely, the cyclic variations of internal engine activity (each flash of the light curve corresponds to one of its four episodes).

The detected non-stationarity of the ejection flow can be a result of non-stationary accretion due to periodically triggered gravitational instability (Masada et al. 2007) in the hot inner part of one solar mass hyperaccreting disk, around a compact object with a mass of about three solar masses, formed in the collapse of a massive star (Woosley 1993; Zhang, Woosley & Heger 2004).

Such a disk must contain a large amount of neutrons (Pruet et al. 2003), and the four peaks detected in the optical light curve reflect the four episodes of accretion activity leading to the ejection of matter. The matter forming the inner part of the disk (fragmented due to instabilities) becomes the elements of the jet. The collisions of these fragments generate the internal shocks in the ejecta. Moreover, the half-second variations in the source frame, marginally seen during the last stage of the optical transient (see Fig. 3c), may be interpreted as a result of the Lense-Thirring precession or nutation (J.Hartle, K.Thorne & R.H.Price 1986; Reynoso, Romero & Sampayo 2006) of the inner parts of this disk.

5. Conclusions

The strategy of a wide-field monitoring with high temporal resolution (Karpov et al. 2010; Beskin et al. 2010), implemented in the TORTORA camera, made it possible to perform, for the first time, a detailed investigation of the optical flash accompanying GRB 080319B.

We discovered the periodic variability of its optical emission with a characteristic time scale of 8.5 s (4.2 s in source frame), manifested in the four similar light curve peaks. The amplitude of stochastic variations does not exceed 10-15% on the 0.1-1 s time scale, in contrast to highly variable gamma-ray emission. The comparison of light curves reveals a 2 s delay between the optical and the gamma-ray emission, clear despite of a similarity between the overall temporal structures. Correspondingly shifted light curves have a correlation coefficient of $r = 0.82$ over the $T+10$ s – $T+47$ s interval.

The acquired data and their analysis led us to the following conclusions:

- the emission of GRB 080319B in the optical and gamma-ray ranges is generated in different regions of the ejecta, which clearly contradicts a number of models suggested as an explanation of this burst (Racusin et al. 2008; Kumar & Panaitescu 2008; Fan & Piran 2008; Yu et al. 2009; Kumar & Narayan 2009);
- peculiarities of the optical emission variations in comparison to the gamma-ray ones can naturally be explained in the framework of models with either residual collisions of shells (Li & Waxman 2008) or significant neutron component in the outflow (Fan et al. 2009). As the latter model provides a better explanation of various aspects of the observational features of the burst, we suggest the presence of vast amount of neutrons in the jet;
- the four peaks characterizing the optical light curve reflect the periodic modulation of the accretion from the massive disk around the newborn compact object, formed in the core-collapse of a massive star.

Our important data on the detailed structure of GRB 080319B optical emission, never acquired before, suggest that the development of methods and instruments for wide-field monitoring with high temporal resolution should continue. The most important aspect of this kind of instrumentation is the construction of instruments not only able to detect an optical transient, but also able to simultaneously acquire the spectral and polarimetric information from optical photons in real time (Beskin et al. 2010).

Acknowledgments

This work was supported by the Bologna University Progetti Pluriennali 2003, by grants of CRDF (No. RP1-2394-MO-02), RFBR (No. 04-02-17555, 06-02-08313 and 09-02-12053, 12-02-00743-a), INTAS (04-78-7366) and by the Presidium of the Russian Academy of Sciences Program and by the grant of President of Russian Federation for the support of young Russian scientists. S. K. has also been supported by a grant of Dynasty foundation. G. B. thanks Landau Network-Cenro Volta and Cariplo Foundation for fellowship and Brera Observatory for hospitality. G. G. also gratefully

acknowledges the support of Foundatione CARISBO. We thank Emilio Molinari, Stefano Covino and Cristiano Guidorzi for technical help organizing TORTORA observations and for discussions of the results.

References

Akerlof C., Balsano R., Barthelmy S., et al., 1999, Nature, 398, 400
Bersier D., Stanek K. Z., Winn J. N., et al., 2003, ApJL, 584, L43
Beskin G., Karpov S., Bondar S., et al., 2008, in Huang Y.-F., Dai Z.-G., Zhang B., eds, 2008 Nanjing gamma-ray burst conference, American Institute of Physics Conference Series, 1065, 251
Beskin G., Bondar S., Karpov S., et al., 2010, Advances in Astronomy, 2010, ID 171569
Derishev E. V., Kocharovsky V. V., Kocharovsky V. V., 1999, ApJ, 521, 640
Fan Y.-Z., Piran T., 2008, Frontiers of Physics in China, 3, 306
Fan Y.-Z., Zhang B., Wei D.-M., 2009, Phys. Rev. D, 79, 021301
Jakobsson P., Hjorth J., Ramirez-Ruiz E., et al., 2004, New Astronomy, 9, 435
Hartle J., Thorne K., Price R. H., 1986, in Thorne K., Price R., MacDonald D., eds, Black Holes: the Membrane Paradigm New Haven, Yale University Press, chap. 5, 173
Karpov S., Beskin G., Biryukov, A., et al., 2005, Nuovo Cimento C Geophysics Space Physics C, 28, 747
Karpov S., Beskin G., Bondar S., et al., 2008, GRB Coordinates Network Circular, 7452
Karpov S., Beskin G., Bondar S., et al., 2010, Advances in Astronomy, 2010
Kocevski R., Ryde F., Liang E., 2003, ApJ, 596, 389
Kumar P., Narayan R., 2009, MNRAS, 395, 472
Kumar P., Panaitescu A., 2008, MNRAS, 391, L19
Li Z., Waxman E., 2008, ApJ, 674, 65
Margutti R., Guidorzi C., Chincarini G., et al., 2008, in Huang Y.-F., Dai Z.-G., Zhang B., eds, 2008 Nanjing gamma-ray burst conference, American Institute of Physics Conference Series, 1065, 259
Masada Y., Kawanaka, N., Sano T., et al., 2007, ApJ, 663, 437
Meszaros, P., 2006, Reports on Progress in Physics, 69, 2259
Molinari E., Bondar S., Karpov S., et al., 2006, Nuovo Cimento B, 121, 1525
Page K. L., Willingale R., Osborne J. P., et al. 2007, ApJ, 663, 1125
Piccioni A., Bartolini A., Cosentino C., et al., 1993, in Friedlander M., Gehrels N., Macomb D. J., eds, American Institute of Physics Conference Series, American Institute of Physics Conference Series, 280, 1152
Piran T., 2005, Reviews of Modern Physics, 76, 1143
Pruet J., Woosley S. E., Hoffman R. D., 2003, ApJ, 586, 1254
Racusin J. L., Karpov S. V.; Sokolowski M., et al., 2008, Nature, 455, 183
Reynoso M. M., Romero G. E., Sampayo O. A., 2006, A&A, 454, 11
Vestrand W. T., Wozniak, P. R.; Wren, J. A., et al., 2005, Nature, 435, 178
Woosley S., 1993, ApJ, 405, 273
Yost S. A., Swan H. F., Rykoff E. S., et al., 2007, ApJ, 657, 925
Yu Y. W., Wang X. Y., Dai Z. G., 2009, ApJ, 692, 1662
Zhang W., Woosley S. E., Heger A., 2004, ApJ, 608, 365
Zou Y.-C., Piran T., Sari R., 2009, ApJL, 692, L92